



CHORUS

This is the accepted manuscript made available via CHORUS. The article has been published as:

Spectrum Control through Discrete Frequency Diffraction in the Presence of Photonic Gauge Potentials

Chengzhi Qin, Feng Zhou, Yugui Peng, Dimitrios Sounas, Xuefeng Zhu, Bing Wang, Jianji Dong, Xinliang Zhang, Andrea Alù, and Peixiang Lu

Phys. Rev. Lett. **120**, 133901 — Published 27 March 2018

DOI: [10.1103/PhysRevLett.120.133901](https://doi.org/10.1103/PhysRevLett.120.133901)

Spectrum Control through Discrete Frequency Diffraction in the Presence of Photonic Gauge Potentials

Chengzhi Qin,¹ Feng Zhou,¹ Yugui Peng,¹ Dimitrios Sounas,² Xuefeng Zhu,¹ Bing Wang,^{1,*}
Jianji Dong,^{1,†} Xinliang Zhang,¹ Andrea Alù,^{2,3‡} and Peixiang Lu^{1,4,§}

¹Wuhan National Laboratory for Optoelectronics and School of Physics, Huazhong University of Science and Technology, Wuhan, 430074, China

²Department of Electrical and Computer Engineering, The University of Texas at Austin, Austin, Texas 78712, USA

³Advanced Science Research Center, City University of New York, New York, NY 10031, USA

⁴Laboratory for Optical Information Technology, Wuhan Institute of Technology, Wuhan, 430205, China

E-mails:

* wangbing@hust.edu.cn

† jjdong@hust.edu.cn

‡ aalu@gc.cuny.edu

§ lupeixiang@hust.edu.cn

Abstract

By using optical phase modulators (PMs) in a fiber-optical circuit, we theoretically and experimentally demonstrate large control over the spectrum of an impinging signal, which may evolve analogously to discrete diffraction in spatial waveguide arrays. The modulation phase acts as a photonic gauge potential in the frequency dimension, realizing efficient control of the central frequency and bandwidth of frequency combs. We experimentally achieve a 50 GHz frequency shift and three-fold bandwidth expansion of an impinging comb, as well as the frequency analogue of various refraction phenomena, including negative refraction and perfect focusing in the frequency domain, both for discrete and continuous incident spectra. Our study paves a promising way towards versatile frequency management for optical communications and signal processing using time modulation schemes.

Controlling the frequency of light is important both in exploring fundamental physics [1-5] and for practical applications, ranging from high-speed communication [6, 7], ultrafast spectroscopy [8, 9] to precise metrology [9-11]. Traditional methods to modify and control the frequency content of a signal rely on nonlinear optical effects, as in highly nonlinear fibers [12, 13]. However, nonlinear optical phenomena are limited by intrinsically low efficiencies and require high pump power [14, 15]. Another possibility to achieve frequency conversion is through temporal modulation [16-19], which has raised significant attention recently in the context of non-reciprocal signal propagation [18, 19]. Temporal modulation offers the additional advantage of controlling the phase of light through the generation of an effective gauge potential for photons, in direct analogy with how the vector potential changes the phase of electron wavefunction [20-27]. The effective gauge potential in turn provides new opportunities to control photons, in analogy with how electrons can be controlled by suitably tailored vector potentials, including the realization of photonic Aharonov-Bohm effect [20, 22-24], photonic quantum Hall effect [21] and non-magnetic optical isolators and circulators [22, 25-27].

Here we investigate another opportunity offered by the effective photonic gauge potential in time-modulated systems, consisting in the precise control and manipulation of the spectrum of impinging signals. Towards this goal, we have been inspired by discrete diffraction phenomena in waveguide arrays, which enable efficient control of the spatial profile of optical beams as they propagate along them [28-32]. In this paper, we show that a temporally modulated waveguide can realize analogous diffraction phenomena, with the transverse spatial dimension replaced by a synthetic frequency dimension. The band structure of this synthetic lattice can be efficiently controlled by a photonic gauge potential through different modulation phases, enabling the generation of frequency combs with controllable bandwidth and center frequency. We experimentally demonstrate this effect in a fiber-optic system based on two cascaded optical phase modulators driven by a radiofrequency sinusoidal alternating voltage. By varying the phase of the radiofrequency signal of the two modulators, we can control the photonic gauge potential, and in turn we realize various refraction phenomena and perfect imaging in the synthetic frequency space. All demonstrated phenomena can be applied in optical communications and signal processing systems, where the development of techniques for efficient control of the impinging spectrum is very important.

Consider a travelling-wave electro-optic phase modulator consisting of LiNbO₃ waveguide. As schematically shown in Fig. 1(a), the waveguide is modulated by a sinusoidal radiofrequency (RF) signal with instantaneous refractive index $n(z, t) = n_0 + \Delta n \cdot \cos(\Omega t - qz + \phi)$. Here n_0 is the background refractive index, Δn , Ω , q and ϕ are the modulation amplitude, frequency, wave vector, and initial phase, respectively. The dispersion relation of the considered mode in the vicinity of ω_0 is shown in Fig. 1(b). As the waveguide is modulated by an alternating voltage with frequency Ω , new frequencies in the spectrum are generated through intraband transitions, forming a frequency comb with frequency interval Ω . The electric field of the frequency comb is $E = \sum_n a_n(z) \exp[i(\omega_n t - \beta_n z)]$, where $\omega_n = \omega_0 + n\Omega$ and $\beta_n = \beta_0 + nq$ ($n = 0, \pm 1, \pm 2, \dots$) denote the frequency and propagation constant of n th-order optical mode, respectively. In order to satisfy the phase-matching condition, the group velocity of the optical mode should be equal to the modulation signal velocity [33-35]. Within a narrow frequency range around ω_0 , the dispersion relation of the mode is linear and the group velocity dispersion can be neglected, as shown in Fig. 1(b). The phase-matching condition becomes $\Omega/q = c/n_g$ with n_g being the group index of the mode at ω_0 . The amplitude of the n th-order mode $a_n(z)$ is governed by the coupled-mode equation [36]

$$i \frac{\partial a_n(z)}{\partial z} = C \left(e^{i\phi} a_{n-1}(z) + e^{-i\phi} a_{n+1}(z) \right), \quad (1)$$

where $C = \Delta n k_0 / 2$ is the coupling strength between adjacent order modes with k_0 being the vacuum wavenumber. Equation (1) is mathematically consistent to the equation describing mode coupling in a spatial waveguide array, highlighting the analogy between these two systems, where the transverse spatial dimension of the array is replaced by a synthetic frequency dimension. The additional phase acquired by the optical mode during photonic transitions is equal and opposite to the modulation phase for upward and downward transitions, respectively. Such a nonreciprocal phase shift is the photonic analogue of the electronic Peierls phase $\phi = \int_c A ds$ acquired by an electron as it moves along a path c in the presence of a magnetic vector potential A [20-27, 37-39]. Here the gauge potential operates in the synthetic frequency dimension and is related to the phase of photons when hopping from one frequency to another

$$\int_{\omega_n}^{\omega_{n+1}} A_{\text{eff}} d\omega = \phi, \quad (2)$$

from which we find $A_{\text{eff}} = \phi / \Omega$. Since the definition of ϕ relies on the choice of time origin and

exhibits a gauge ambiguity, the potential is also gauge-dependent. Therefore, the effect of gauge potential is embodied in the gauge-invariant phase difference of modulation as a reference modulation phase.

Similar to spatial waveguide array, the frequency dimension can support Bloch modes with $a_n(z) = a_0(0)\exp(in\phi_0)\exp(ik_z z)$. Here $a_0(0)$ is the uniform amplitude, ϕ_0 is the initial Bloch momentum along frequency dimension and k_z is the collective propagation constant in the z direction. The Bloch mode is itself a frequency comb, with Bloch momentum acting as the phase difference between adjacent comb lines. Substituting $a_n(z)$ into Eq. (1), we can obtain the band structure for the frequency comb

$$k_z(\phi_0) = -2C \cos(\phi_0 - \phi), \quad (3)$$

Denoting $\phi_0 = k_\omega \Omega$, k_ω is the initial Bloch wave vector in the frequency dimension. The band structure is rewritten as $k_z(k_\omega) = -2C \cos[(k_\omega - A_{eff})\Omega]$, so the gauge potential can induce a band structure shift in the momentum space [40, 41]. For a realistic frequency comb with finite width and center Bloch momentum ϕ_0 , the group velocity in frequency dimension is $v_{g,\omega} = -\partial k_z / \partial k_\omega = -2C\Omega \sin(\phi_0 - \phi)$, giving rise to a frequency shift $\Delta\omega(z) = \int_0^z v_{g,\omega} dz'$. For one PM with length L , the phase modulation depth is $m_\phi = \Delta n k_0 L = 2CL$. So the total accumulated frequency shift is

$$\Delta\omega = -m_\phi \Omega \sin(\phi_0 - \phi), \quad (4)$$

In addition to undergoing central spectral shift, the finite-width frequency comb will also experience bandwidth expansion, which can be described by the diffraction coefficient [28-30]

$$D = \frac{\partial^2 k_z}{\partial k_\omega^2} = 2C\Omega^2 \cos(\phi_0 - \phi), \quad (5)$$

which also refers to the group velocity dispersion in frequency space. From Eqs. (4) and (5), we can infer that $|\Delta\omega|_{max} = m_\phi \Omega$ and $|D|_{min} = 0$ for $\phi_0 - \phi = \pm \pi/2$. The frequency comb will experience diffraction-free evolution with maximum spectral shift. On the other hand, for $\phi_0 - \phi = 0$ or π , we have $|\Delta\omega|_{min} = 0$ and $|D|_{max} = 2C\Omega^2$, the spectral shift vanishes and the bandwidth expansion reaches its maximum.

By cascading two PMs with distinct modulation phases ϕ_1 and ϕ_2 , the frequency comb will exhibit a refraction at their boundary, analogous to the refraction at the interface between two mediums with different refractive index. The relative refractive index is $n_{12}(\phi_0) = k_{z,1}(\phi_0)/k_{z,2}(\phi_0)$,

which is given by

$$n_{12}(\phi_0) = \frac{\cos(\phi_0 - \phi_1)}{\cos(\phi_0 - \phi_2)}, \quad (6)$$

By employing different gauge potentials in the two PMs, we can impart arbitrary refraction phenomena on the frequency combs, such as realizing positive, negative refraction and spectral compression.

The above theoretical analysis has been experimentally verified in Fig. 2(a), which consists of two cascaded PMs (PM1 and PM2) with modulation phases ϕ_1 and ϕ_2 . In the implementation, the connector A is switched on. The frequency comb is generated by a mode-locked laser with initial Bloch momentum ϕ_0 , which is synchronized with the two PMs by a fixed modulation frequency $\Omega/2\pi = 10$ GHz. Other experiment details are discussed in Supplementary [36]. Firstly, we keep two PMs modulated in phase ($\phi_1 = \phi_2$) and fix $m_{\phi_1} = m_{\phi_2}$. As shown in Fig. 2(b), the envelope of frequency comb experiences a sinusoidal variation as $\phi_0 - \phi_1$ varies. The continuous evolution of frequency shift is due to the variation of gauge potential, which agrees well with the theoretical prediction of Eq. (4). The spectrum can also be controlled by the modulation depth $m_\phi (= m_{\phi_1} + m_{\phi_2})$. In the experiment, the modulation is first applied on PM1 and the modulation depth m_{ϕ_1} increases linearly to its maximum. Then we fix m_{ϕ_1} and increase linearly the modulation depth m_{ϕ_2} on PM2 until its maximum with the same value of m_{ϕ_1} , as shown in the inset of Fig. 2(a). In Figs. 2(c) and 2(d), the spectral width remains constant and the comb center manifests linear blue and red shifts for $\phi_0 - \phi_1 = -\pi/2$ and $\pi/2$, respectively. The maximum frequency shift is ~ 50 GHz (~ 0.4 nm) which spans up to five comb lines. On the other hand, for $\phi_0 - \phi_1 = 0$ in Fig. 2(e), the spectral center is not affected and bandwidth is broadened by three folds from 0.18 to ~ 0.6 nm. Again, these results are fully consistent with theoretical predictions. Finally, by applying distinct gauge potentials to the two PMs, such that $\phi_1 \neq \phi_2$, we can impart arbitrary refraction phenomena for the frequency comb. In Fig. 2(f), we choose $\phi_0 - \phi_1 = -\pi/2$ and $\phi_0 - \phi_2 = \pi/2$, the frequency comb undergoes a “negative refraction” between the two PMs. Other scenarios of frequency refractions are shown in Supplementary Fig. (S5) [36].

In addition to enabling the diffraction control of frequency combs, the gauge potentials can also provide broad control over frequency comb generation. For one PM under a single frequency input, the output spectrum is $a_n = a_0(i)^n J_n(m_\phi) \exp(in\phi)$, where a_0 is the input amplitude and J_n is n th-order

Bessel function. Since the definition of ϕ relies on the choice of time origin, it has no physical meaning on its own without reference and cannot be detected from the output amplitude spectrum $|a_n| = a_0|J_n(m_\phi)|$. On the contrary, for two cascaded PMs under a single frequency input, the output amplitude spectrum is [36]

$$|a_n| = a_0 |J_n(2m_{\phi_1} \cos(\frac{\Delta\phi}{2}))|, \quad (7)$$

Where $m_{\phi_1} = m_{\phi_2}$, $\Delta\phi = \phi_2 - \phi_1$. Therefore, the phase difference of modulation is gauge-invariant and can be utilized to control the frequency comb generation.

We have verified this phenomenon experimentally by using a continuous-wave laser (connector B in Fig. 2(a) is switched on) to generate a single frequency. Firstly, we keep $m_{\phi_1} = m_{\phi_2}$ and vary $\Delta\phi = \phi_2 - \phi_1$ from 0 to π , as shown in Fig. 3(a), the output spectrum is squeezed from its maximum to a single frequency, validating the theoretical prediction of Eq. (7). We can also fix $\Delta\phi$ and successively increase m_{ϕ_1} and m_{ϕ_2} . The band structures of the two PMs are shown in Fig. 3(b) as $\phi_1 = \pi/2$, $\phi_2 = -\pi/2$. For in-phase modulation $\Delta\phi = 0$, shown in Fig. 3(c), the output spectrum is $|a_n| = a_0|J_n(m_{\phi_1} + m_{\phi_2})|$, which exhibits constructive interference of frequency comb generation in the two PMs. On the other hand, for out-of-phase modulation $\Delta\phi = \pi$, as shown in Fig. 3(d), the output spectrum becomes $|a_n| = a_0|J_n(m_{\phi_1} - m_{\phi_2})|$, manifesting destructive interference of comb generation in the two PMs. Interestingly as $m_{\phi_1} = m_{\phi_2}$, the spectrum exhibits a time-reversal process in PM2 and ultimately restores to the input single-frequency, manifesting the analogue of “perfect imaging” in the frequency domain.

The signal of a single-frequency can be regarded as the superposition of all frequency combs with Bloch momentum ϕ_0 covering the entire Brillouin zone. For $\Delta\phi = \pi$ in Fig. 3(b), the band structures exhibit opposite shift with $n_{12}(\phi_0) = -1$, each frequency comb exhibits negative refraction and opposite phase front evolutions in the two PMs [36], giving rise to the perfect focusing for a single-frequency. This phenomenon is analogous to the perfect imaging of a point light source by a real-space “superlens” [42-45]. The two PMs with $\Delta\phi = \pi$ can be treated as a frequency “superlens”, with a relative refractive index of $n_{12} = -1$. Interestingly, this frequency “superlens” does not require complicated metamaterials devices, it can be flexibly constructed by out-of-phase modulation of two PMs.

The phenomenon of “perfect imaging” in the frequency domain is applicable to arbitrary input

spectra. In Figs. 4(a)-4(c), we input two continuous-wave lasers of 1550 and 1550.08 nm, with frequency interval $\Omega/2\pi = 10$ GHz. In Fig. 4(a), the output spectrum is squeezed from the widest to its original input of two frequencies as $\Delta\phi$ varies from 0 to π . For $\Delta\phi = 0$ in Fig. 4(b), the input two frequencies exhibit linear diffraction as m_ϕ increases, forming a broad frequency comb. For $\Delta\phi = \pi$ in Fig. 4(c), the spectrum experiences discrete diffraction in PM1 and restore to its initial profile at the end of PM2. In Figs. 4(d)-4(f), the incident wave is a supercontinuum spectrum [46], as the connector C in Fig. 2(b) is switched on. In Fig. 4(d), the output spectral width is squeezed monotonously as $\Delta\phi$ varies. For $\Delta\phi = 0$ shown in Fig. 4(e), the spectrum is linearly broadened as m_ϕ increases. While for $\Delta\phi = \pi$ in Fig. 4(f), the spectrum is broadened in PM1 and then compressed in PM2, ultimately being restored to its initial profile. The results confirm that the perfect imaging can be applied to arbitrary discrete and continuous spectra, see also Supplementary Fig. (S7) [36].

Finally, we investigate the nonreciprocal properties of discrete frequency diffraction in the system, enabled by the time-reversal symmetry breaking through temporal modulation. In Figs. 5(a) and 5(b), we inject a single frequency into one PM in forward and backward directions and vary the modulation frequency from $\Omega/2\pi = 6$ GHz to 18 GHz. As the waves propagate forward, the frequency comb can be generated with the interval being equal to the modulation frequency. While in the backward, the side bands of output spectrum are negligible. The nonreciprocal property is attributed to the phase-matching condition required to induce photonic transitions. As the RF and optical waves propagate in opposite directions, the phase-matching condition is destroyed and photonic transitions are negligible. These results suggest that discrete frequency diffraction can exhibit inherent nonreciprocal properties over a broad bandwidth.

In summary, we demonstrate discrete frequency diffraction in temporal modulated waveguides, which is analogous to discrete diffraction of light in spatial waveguide arrays. The spectral shift and bandwidth expansion for frequency combs can be arbitrarily controlled by photonic gauge potentials originating from the modulation phase. A frequency shift up to 50 GHz and bandwidth expansion up to three-folds for frequency combs have been achieved. These metrics can be further improved by using more PMs. By cascading two PMs with distinct gauge potentials, we also realize negative refraction for frequency combs and perfect imaging for arbitrary input spectra. Our study may stimulate the developments of high-efficient frequency shifters and perfect-lens, with applications in signal reshaping, spectral-temporal imaging, and secure optical communications.

The work is supported by the 973 Program (No. 2014CB921301), the National Natural Science Foundation of China (Nos. 11674117, 61622502, 11690030, 11690032), the Simons Foundation, the National Science Foundation and the Air Force Office of Scientific Research.

C. Qin, F. Zhou, and Y. Peng contributed equally to this work.

References

- [1] S. Zaske *et al.*, Phys. Rev. Lett. **109**, 147404 (2012).
- [2] S. Ates, I. Agha, A. Gulinatti, I. Rech, M. T. Rakher, A. Badolato, and K. Srinivasan, Phys. Rev. Lett. **109**, 147405 (2012).
- [3] J. Lavoie, J. M. Donohue, L. G. Wright, A. Fedrizzi, and K. J. Resch, Nat. Photonics **7**, 363 (2013).
- [4] M. Karpiński, M. Jachura, L. J. Wright, and B. J. Smith, Nat. Photonics **11**, 53 (2016).
- [5] T. Kobayashi, R. Ikuta, S. Yasui, S. Miki, T. Yamashita, H. Terai, T. Yamamoto, M. Koashi, and N. Imoto, Nat. Photonics **10**, 441 (2016).
- [6] I. B. Djordjevic and B. Vasic, Opt. Express **14**, 3767 (2006).
- [7] J. Pfeifle *et al.*, Nat. Photonics **8**, 375 (2014).
- [8] D. R. Solli, J. Chou, and B. Jalali, Nat. Photonics **2**, 48 (2008).
- [9] K. Goda and B. Jalali, Nat. Photonics **7**, 102 (2013).
- [10] T. Udem, R. Holzwarth, and T. W. Hänsch, Nature (London) **416**, 233 (2002).
- [11] A. Schliesser, N. Picqué, and T. W. Hänsch, Nat. Photonics **6**, 440 (2012).
- [12] C. Bersch, G. Onishchukov, and U. Peschel, Opt. Lett. **34**, 2372 (2009).
- [13] C. Bersch, G. Onishchukov, and U. Peschel, Appl. Phys. B **104**, 495 (2011).
- [14] R. W. Boyd, *Nonlinear optics* (Academic Press, San Diego, 2003).
- [15] G. P. Agrawal, *Nonlinear Fiber Optics* (Academic Press, New York, 2001).
- [16] X. Guo, C. L. Zou, H. Jung, and H. X. Tang, Phys. Rev. Lett. **117**, 123902 (2016).
- [17] L. Fan, C.-L. Zou, M. Poot, R. Cheng, X. Guo, X. Han, and H. X. Tang, Nat. Photonics **10**, 766 (2016).
- [18] Z. Yu and S. Fan, Nat. Photonics **3**, 91 (2009).
- [19] D. Sounas, A. Alù, Nat. Photonics **11**, 774 (2017).
- [20] K. Fang, Z. Yu, and S. Fan, Phys. Rev. Lett. **108**, 153901 (2012).
- [21] K. Fang, Z. Yu, and S. Fan, Nat. Photonics **6**, 782 (2012).
- [22] L. D. Tzuan, K. Fang, P. Nussenzveig, S. Fan, and M. Lipson, Nat. Photonics **8**, 701 (2014).
- [23] E. Li, B. J. Eggleton, K. Fang, and S. Fan, Nat. Commun. **5**, 3225 (2014).
- [24] C. Qin, B. Wang, H. Long, K. Wang, and P. Lu, J. Lightwave Technol. **34**, 3877 (2016).
- [25] N. A. Estep, D. L. Sounas, J. Soric, and A. Alù, Nat. Phys. **10**, 923 (2014).

- [26] D. L. Sounas and A. Alù, *ACS photonics* **1**, 198 (2014).
- [27] K. Fang, J. Luo, A. Metelmann, M. H. Matheny, F. Marquardt, A. A. Clerk, and O. Painter, *Nat. Phys.* **14**, 465 (2017).
- [28] H. S. Eisenberg, Y. Silberberg, R. Morandotti, and J. S. Aitchison, *Phys. Rev. Lett.* **85**, 1863 (2000).
- [29] T. Pertsch, T. Zentgraf, U. Peschel, A. Bräuer, and F. Lederer, *Phys. Rev. Lett.* **88**, 093901 (2002).
- [30] D. N. Christodoulides, F. Lederer, and Y. Silberberg, *Nature (London)* **424**, 817 (2003).
- [31] B. Wang, X. Zhang, F. J. García-Vidal, X. Yuan, and J. Teng, *Phys. Rev. Lett.* **109**, 073901 (2012).
- [32] A. Block, C. Etrich, T. Limboeck, F. Bleckmann, E. Soergel, C. Rockstuhl, and S. Linden, *Nat. Commun.* **5**, 3843 (2014).
- [33] W. S. Chang, *RF Photonic Technology in Optical Fiber Links* (Cambridge University Press, New York, 2002).
- [34] H. Murata, A. Morimoto, T. Kobayashi, and S. Yamamoto, *IEEE J. Sel. Top. Quant. Elec.* **6**, 1325 (2000).
- [35] H. V. Pham, H. Murata, and Y. Okamura, *Advance in OptoElectronics* **2008**, 1 (2008).
- [36] See Supplementary Material for more details on the derivation of the coupled-mode equations and frequency comb generation by optical phase modulators, the experimental setup and measurement, and additional simulation results of frequency evolution.
- [37] J. Dalibard, F. Gerbier, G. Juzeliūnas, and P. Öhberg, *Rev. Mod. Phys.* **83**, 1523 (2011).
- [38] K. Jimenez-Garcia, L. J. LeBlanc, R. A. Williams, M. C. Beeler, A. R. Perry, and I. B. Spielman, *Phys. Rev. Lett.* **108**, 225303 (2012).
- [39] L. Lu, J. D. Joannopoulos, and M. Soljačić, *Nat. Photonics* **8**, 821 (2014).
- [40] K. Fang and S. Fan, *Phys. Rev. Lett.* **111**, 203901 (2013).
- [41] L. Yuan and S. Fan, *Phys. Rev. Lett.* **114**, 243901 (2015).
- [42] J. B. Pendry, *Phys. Rev. Lett.* **85**, 3966 (2000).
- [43] N. Fang, H. Lee, C. Sun, and X. Zhang, *Science* **308**, 534 (2005).
- [44] T. Xu, A. Agrawal, M. Abashin, K. J. Chau, and H. J. Lezec, *Nature (London)* **497**, 470 (2013).
- [45] R. Fleury, D. L. Sounas, and A. Alù, *Phys. Rev. Lett.* **113**, 023903 (2014).

[46] J. M. Dudley, G. Genty, and S. Coen, *Rev. Mod. Phys.* **78**, 1135 (2006).

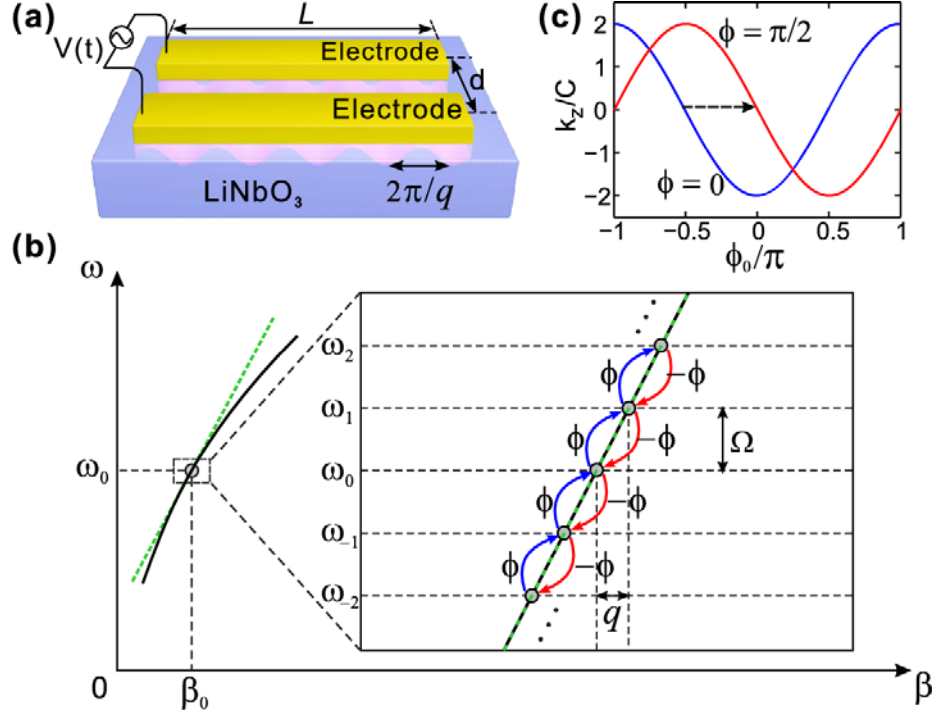


FIG. 1. (a) Schematic of LiNbO₃ phase modulator (PM), modulated by a travelling-wave RF signal through two parallel electrodes with length L and spacing d . (b) Dispersion curve of optical modes and photonic intraband transitions in the vicinity of ω_0 . The green dashed line denotes the tangent of the dispersion curve at ω_0 . Ω , q are the modulation frequency and wave vector with $\pm \phi$ being the phase shift accompanying photonic transitions. (c) Band structure of frequency comb for $\phi = 0$ and $\phi = \pi/2$.

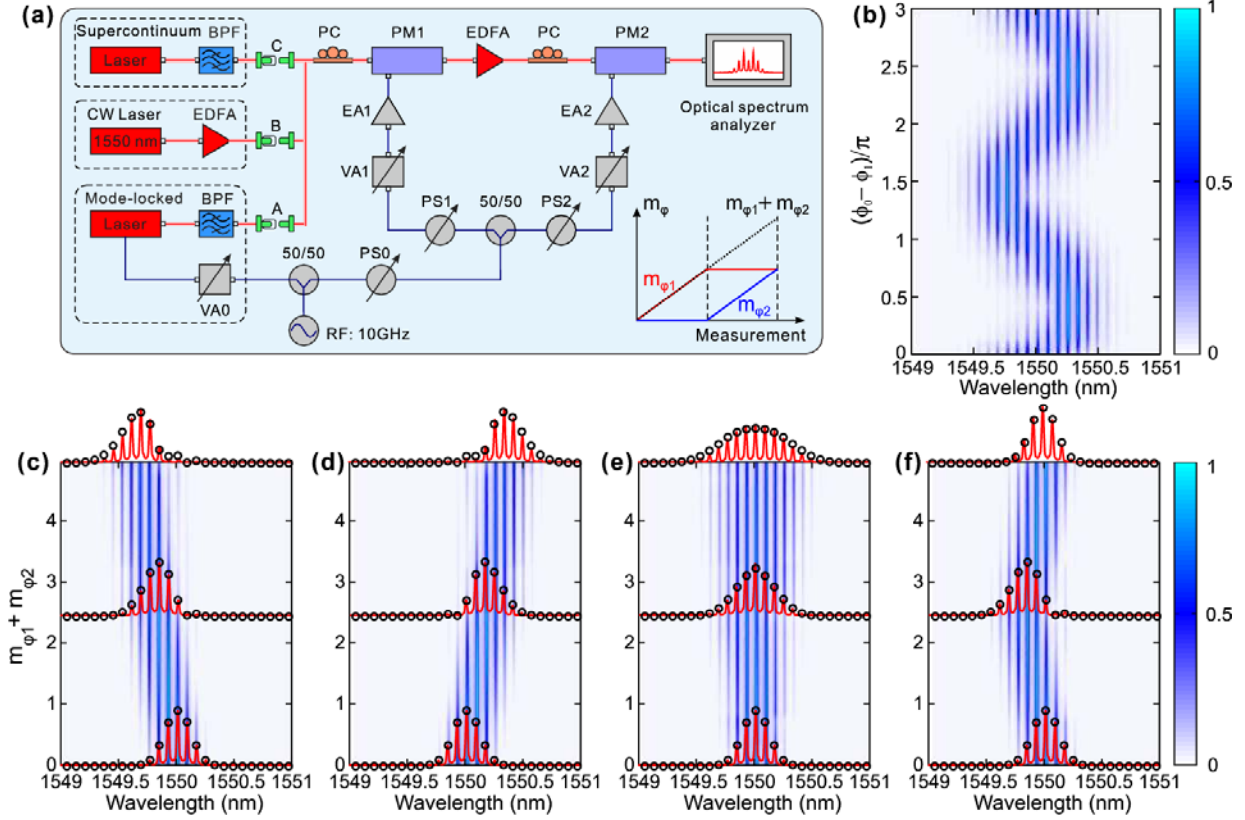


FIG. 2. (a) Experimental set-up. PS: phase shifter, EA: electrical amplifier, VA: variable attenuator, BPF: band-pass filter, PC: polarizer controller, EDFA: erbium-doped fiber amplifier. Different optical sources are utilized separately when only one of the fiber connectors A, B, and C is switched on in each experimental implementation. Inset depicts the process of varying modulation depth m_{ϕ_1} and m_{ϕ_2} upon the two PMs, respectively. (b) Output frequency spectrum as $\phi_0 - \phi_1$ varies for $m_{\phi_1} = m_{\phi_2}$. (c)-(e) Frequency comb evolution as $\phi_0 - \phi_1 = -\pi/2, \pi/2,$ and 0 for $\phi_1 = \phi_2$. (f) Frequency comb evolutions for $\phi_0 - \phi_1 = -\pi/2$ and $\phi_0 - \phi_2 = \pi/2$.

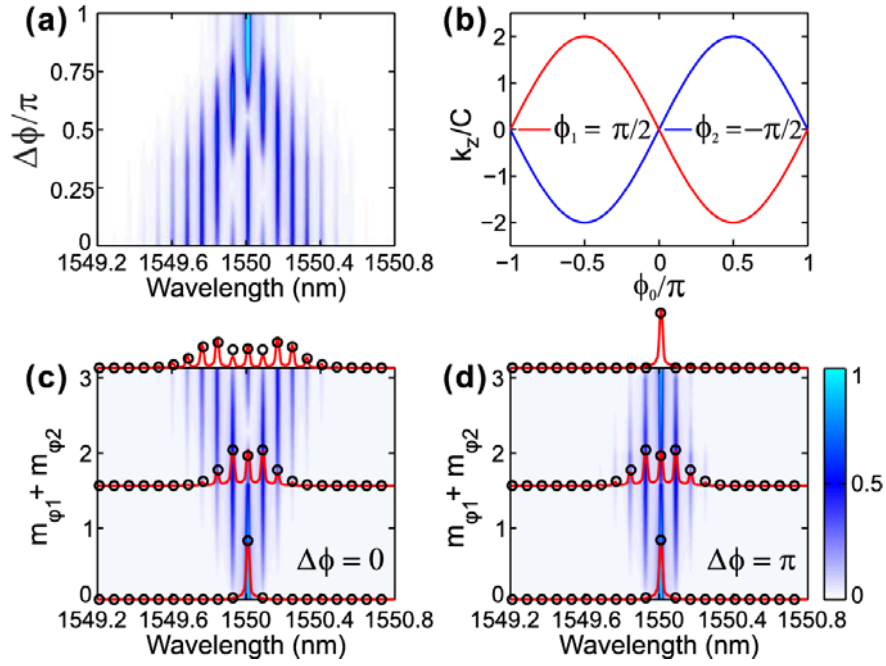


FIG. 3. (a) Output frequency spectrum versus $\Delta\phi$ for $m_{\phi_1} = m_{\phi_2}$. (b) Band structures of the two PMs for $\phi_1 = -\pi/2$ and $\phi_2 = \pi/2$. Frequency evolutions: (c) $\Delta\phi = 0$. (d) $\Delta\phi = \pi$.

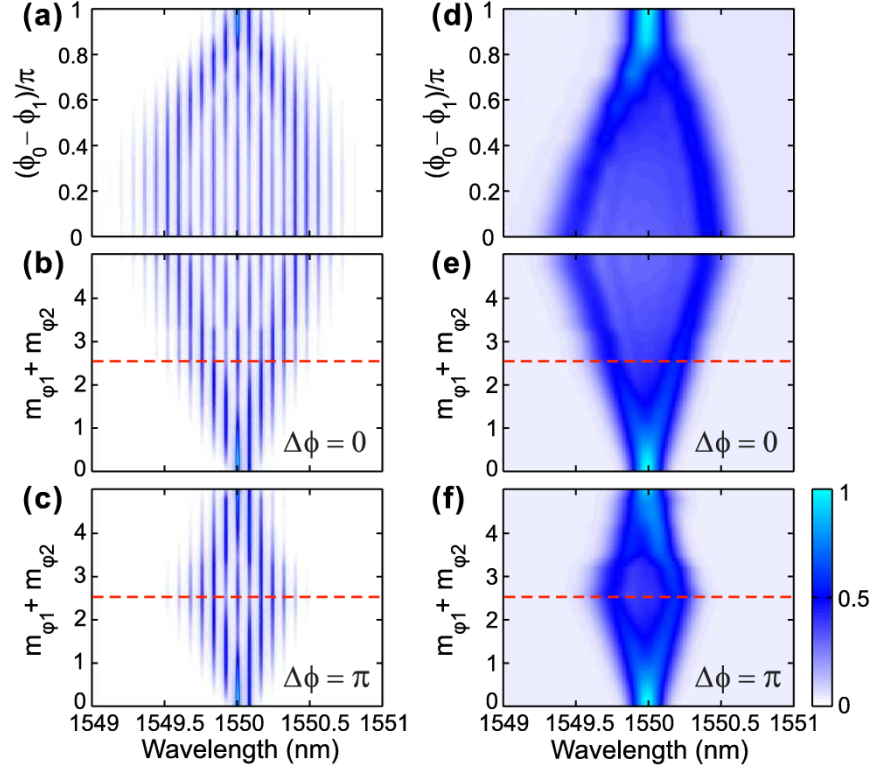


FIG. 4. (a) Two continuous-wave laser evolution versus $\Delta\phi$ for $m_{\phi_1} = m_{\phi_2}$. Output spectral evolutions: (b) $\Delta\phi = 0$. (c) $\Delta\phi = \pi$. (d) Supercontinuum evolution versus $\Delta\phi$ for $m_{\phi_1} = m_{\phi_2}$. Supercontinuum evolutions: (e) $\Delta\phi = 0$. (f) $\Delta\phi = \pi$. The red dashed lines denote the maximum modulation depth applied on PM1.

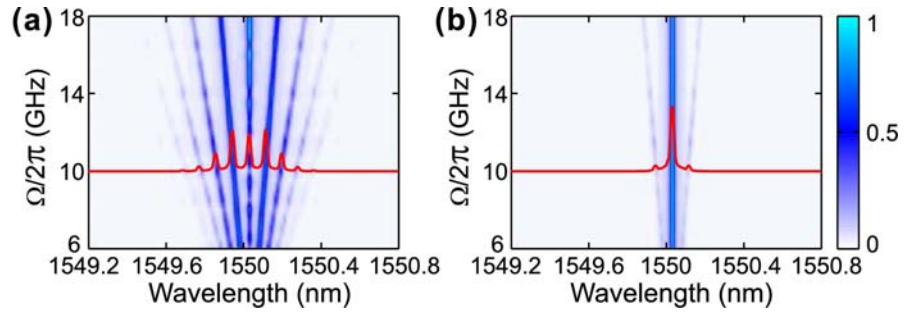


FIG. 5. Output spectral evolution of one PM versus the modulation frequency under a single-frequency input from forward (a) and backward (b) directions. The red lines indicate the output spectra as $\Omega/2\pi = 10$ GHz.